

Photoelectron spectroscopy and dissociative photoionization of fulminic acid, HCNO

Accepted Manuscript: This article has been accepted for publication and undergone full peer review but has not been through the copyediting, typesetting, pagination, and proofreading process, which may lead to differences between this version and the Version of Record.

Cite as: J. Chem. Phys. (in press) (2023); <https://doi.org/10.1063/5.0142194>

Submitted: 12 January 2023 • Accepted: 13 February 2023 • Accepted Manuscript Online: 13 February 2023

 Marius Gerlach,  Barry P. Mant, Tobias Preitschopf, et al.



View Online



Export Citation



CrossMark

ARTICLES YOU MAY BE INTERESTED IN

[Threshold photoelectron spectroscopy of the methoxy radical](#)

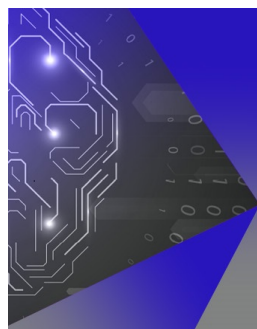
The Journal of Chemical Physics **153**, 031101 (2020); <https://doi.org/10.1063/5.0016146>

[Photoionization spectroscopy of the SiH free radical in the vacuum-ultraviolet range](#)

The Journal of Chemical Physics **157**, 014303 (2022); <https://doi.org/10.1063/5.0094863>

[Resonances in nitrobenzene probed by the electron attachment to neutral and by the photodetachment from anion](#)

The Journal of Chemical Physics **157**, 064302 (2022); <https://doi.org/10.1063/5.0101358>



APL Machine Learning

Machine Learning for Applied Physics
Applied Physics for Machine Learning

**First Articles
Now Online!**

Photoelectron spectroscopy and dissociative photoionization of fulminic acid, HCNO

Marius Gerlach,¹ Barry Mant,² Tobias Preitschopf,¹ Emil Karaev,¹ Dennis Mayer,³ Heidy M. Quitián-Lara,^{1,4} Patrick Hemberger,⁵ John Bozek,⁶ Graham Worth,^{2, a)} and Ingo Fischer^{1, b)}

¹⁾*Institute of Physical and Theoretical Chemistry, University of Würzburg, 97074 Würzburg, Germany*

²⁾*Department of Chemistry, University College London, London WC1H 0AJ, U.K.*

³⁾*Deutsches Elektronen-Synchrotron (DESY), 22607 Hamburg, Germany*

⁴⁾*present adress: Centre for Astrophysics and Planetary Science (CAPS), School of Physics and Astronomy, University of Kent, Canterbury CT2 7NH, UK*

⁵⁾*Laboratory for Synchrotron Radiation and Femtochemistry, Paul Scherrer Institut (PSI), 5232 Villigen, Switzerland*

⁶⁾*Synchrotron SOLEIL, 91192 Gif-sur-Yvette, France*

(Dated: 10 February 2023)

We report a joint experimental and computational study of the photoelectron spectroscopy and the dissociative photoionization of fulminic acid, HCNO. The molecule is of interest to astrochemistry and astrobiology as a potential precursor of prebiotic molecules. Synchrotron radiation was used as the photon source. Dispersive photoelectron spectra were recorded from 10 eV to 22 eV, covering four band systems in the HCNO cation and an ionization energy of 10.83 eV was determined. Transitions into the Renner-Teller distorted $X^{+2}\Pi$ state of the cation were simulated using wavepacket dynamics based on a vibronic coupling Hamiltonian. Very good agreement between experiment and theory is obtained. While the first excited state of the cation shows only a broad and unstructured spectrum, the next two higher states exhibit a well-resolved vibrational progression. Transitions into the excited electronic states of HCNO⁺ were not simulated, due to the large number of electronic states that contribute to these transitions. Nevertheless, a qualitative assignment is given, based on the character of the orbitals involved in the transitions. The dissociative photoionization was investigated by photoelectron-photoion coincidence spectroscopy. The breakdown diagram shows evidence for isomerization from HCNO⁺ to HNCO⁺ on the cationic potential energy surface. Zero Kelvin appearance energies for the daughter ions HCO⁺ and NCO⁺ have been derived.

I. INTRODUCTION

Fulminic acid, HCNO has been and still is a molecule of considerable interest in organic chemistry.^{1,2} At present, the astrochemical relevance drives spectroscopic and theoretical work on the molecule, because HCNO contains the basic atoms of organic chemistry. It has been detected in numerous astrophysical objects, including molecular clouds, protostars, starless cores such as B1, L1544, and L183, as well as the low-mass star-forming region L1527.^{3–8} It is most likely formed from $\text{CH}_2 + \text{NO} \rightarrow \text{HCNO} + \text{H}$ in the gas phase or $\text{H} + \text{CNO} \rightarrow \text{HCNO}$ on grains.^{9,10} HCNO has three additional stable isomers; isocyanic acid (HNCO), cyanic acid (HOCN) and isofulminic acid (HONC). The relative stability is $\text{HNCO} > \text{HOCN} > \text{HCNO} > \text{HONC}$ with HNCO being the most stable isomer.¹¹ Of these molecules, only isofulminic acid has not yet been detected in interstellar space,⁴ although its microwave spectrum is known.

Given the importance of HCNO in astrochemistry, it is not surprising that significant work has been dedicated to this molecule. Due to its small size HCNO and its isomers have been investigated by various high-level quantum chemical approaches.^{11–17} Bunker *et al.* used the semirigid bender Hamiltonian to fit the remarkably flat potential of the

HCN bending mode,¹⁸ which even inspired two limericks which are included in a review on quasilinear and quasiplanar molecules by Bunker.¹⁹ Particularly relevant for the present work are studies by Mondal *et al.*²⁰ on the appearance of Jahn-Teller and Renner-Teller interactions in HCNO⁺ as well as the work by Luna *et al.* who published the global potential energy surface of the $[\text{H,C,N,O}]^+$ system using density functional theory.²¹ Experimentally the microwave^{22–24} and IR-spectra^{24–32} have been reported, the photodissociation has been investigated at 248 nm³³ and 193 nm³⁴ and the kinetics of the HCNO + OH reaction has been studied³⁵. In the soft X-ray regime, we recently reported normal and resonant Auger spectra of HCNO at all three K-edges.³⁶ In contrast, valence photoelectron spectra have only been reported using He I and II ionization.³⁷ An adiabatic ionization energy $IE_{ad}=10.83$ eV has been derived and transitions into electronically excited states of the ion have been observed. However, band assignments were based on rather simple computations and the Renner-Teller effect in the $X^{+2}\Pi$ ground state of HCNO⁺ was not considered. Hop *et al.* investigated the products formed through electron impact ionization.³⁸ The main dissociation products were m/z 30 and m/z 27 as well as a large number of other products with smaller intensities. Due to the limitations of their setup they were not able to provide energy selective data or provide insights into the mechanism of the dissociation. In this joint experimental and computational study we therefore reinvestigate the photoionization and dissociative photoionization of HCNO by photoelectron spectroscopy using synchrotron radiation and coupled-

^{a)}Electronic mail: g.a.worth@ucl.ac.uk

^{b)}Electronic mail: ingo.fischer@uni-wuerzburg.de

cluster calculations. When combined with high-level computations, photoelectron spectroscopy has shown to be an excellent tool to characterize the electronic structure of reactive molecules,³⁹ as shown for example in recent work on C₄H₄, the paradigm for antiaromaticity.⁴⁰ Note that the photoionization of the isomer isocyanic acid, HNCO has already been extensively investigated by our group.^{41,42}

II. EXPERIMENTAL AND COMPUTATIONAL METHODS

A. Experimental

The photoelectron spectrum was recorded at the soft X-ray beamline PLEIADES⁴³ of Synchrotron SOLEIL, while the breakdown diagram for the analysis of dissociative photoionization was obtained at the VUV beamline of the Swiss Light Source (SLS) in Villigen.⁴⁴ Fulminic acid was prepared according to the procedure by Wentrup *et al.*⁴⁵ Details on the synthesis are given in the supporting information (SI).

At the PLEIADES beamline the HCNO sample enters a gas cell through an effusive inlet. Here, it interacts with the synchrotron light, which is produced by an Apple II HU256 undulator and monochromatized by 400 lines mm⁻¹ grating. The photon energy was fixed at 30 eV and the light was circularly polarized. Since the undulator cannot produce light oriented at the magic angle relative to the detector at this low energy, circularly polarized light was used to avoid anisotropy of the emitted electrons. Electrons entered a VG Scienta R4000 hemispherical electron analyzer through an entrance slit of 300 micrometers. A pass energy of 5 eV was adjusted, leading to a spectral resolution of 6 meV. Electron binding energies E_B are obtained by subtracting the photoelectron kinetic energy from the photon energy $h\nu$:

$$E_B = h\nu - E_{kin}. \quad (1)$$

Error bars in the photoelectron spectra are derived from the full width half maximum of the peak.

At the VUV beamline⁴⁴ the sample also enters the experimental chamber through an effusive inlet. A bending magnet delivers the synchrotron radiation, which is monochromatized using a 150 lines mm⁻¹ grating. Electrons and ions were detected in coincidence by a multi-start/multi-stop scheme by a pair of position sensitive Roentdeck DL40 detectors with a delay line anode.⁴⁶ Threshold electrons were collected with a resolution of 5 meV, the contributions of hot electrons were subtracted according to the procedure of Sztaray and Baer.⁴⁷ The breakdown diagram is produced by dividing the threshold electron signal of each relevant mass channel by the sum of all relevant mass channels. It was recorded from 11.5 to 13.5 eV with 25 meV step size and from 13.5 to 15.3 eV with 20 meV step size.

B. Computational

The equilibrium structures of neutral fulminic acid and the fulminic acid cation were calculated using Molpro⁴⁸⁻⁵⁰

at the CCSD(T)/cc-pVTZ and RCCSD(T)/cc-pVTZ levels of theory⁵¹⁻⁵³, respectively. Both molecules were restricted to be linear. Harmonic vibrational normal modes and frequencies were calculated at optimized geometries using the same methods.

We initially intended to simulate the full experimental photoelectron spectra of fulminic acid, however, it was found that at least 12 electronic states of the molecule spanned the energy range of experiments (see discussion in the SI). The excited state potential energy surfaces were also found to vary in a complicated way along the normal mode coordinates such that they could not be described using a vibronic coupling model. Here we restrict simulation of the photoelectron spectra to the first two electronic states of the fulminic acid cation.

Ab initio energies for the fulminic acid cation were calculated using OpenMolcas⁵⁴ along 1D and 2D cuts of each (neutral) normal mode from the equilibrium geometry outwards using a two state-averaged restricted active space self consistent field⁵⁵ (RASSCF) method followed by second order multi-configurational perturbation theory^{56,57} (CASPT2). The active space comprised of 11 electrons in 10 orbitals (11,10). For the neutral molecule a cc-pVDZ basis was used while for the cation a cc-pVTZ basis was employed. These calculations were based on an initial unrestricted Hartree-Fock treatment at the equilibrium geometry and RASSCF orbitals from the previous geometry were used as starting orbitals for each subsequent geometry. Symmetry was turned off for all calculations and a level shift of 0.2 hartree was used for CASPT2 calculations.

To obtain coupled potential energy surfaces for dynamics calculations and spectra simulations, a vibronic coupling Hamiltonian model⁵⁸ was employed. The diabatic potentials are expressed as a Taylor series, in dimensionless (mass-frequency scaled) normal modes around a particular point, \mathbf{Q}_0 , here taken as the equilibrium geometry. The Hamiltonian can be written in matrix form as

$$\mathbf{H} = \mathbf{H}^{(0)} + \mathbf{W}^{(0)} + \mathbf{W}^{(1)} + \dots \quad (2)$$

with the zeroth-order diagonal Hamiltonian $\mathbf{H}^{(0)}$ often expressed in the harmonic approximation

$$H_{ii}^{(0)} = \sum_{\alpha} \frac{\omega_{\alpha}}{2} \left(\frac{\partial}{\partial Q_{\alpha}} + Q_{\alpha} \right). \quad (3)$$

The subsequent matrices include the effects of electronic excitation and vibronic coupling as a Taylor expansion around \mathbf{Q}_0 . The zero order term $\mathbf{W}^{(0)}$ is a diagonal matrix of excitation energies. The first order term $\mathbf{W}^{(1)}$ usually contains on-diagonal linear terms for each electronic state and off-diagonal linear terms coupling states along a particular mode, however, for fulminic acid these terms are absent due to symmetry.

As discussed in the SI, for all modes the basic harmonic potential was replaced by polynomial or Morse functions which provide more accurate fits to the *ab initio* energies and give better agreement between the calculated and experimental photoelectron spectra.

As the fulminic acid cation is a tetra-atomic linear molecule with C_{∞v} symmetry and degenerate electronic states at equilibrium, it displays the Renner-Teller (RT) effect for the pairs

of degenerate vibrations $Q_{1/2}$ and $Q_{3/4}$. These modes do not have the correct symmetry to provide linear coupling ($\mathbf{W}^{(1)}$) between the electronic states and coupling is provided through second order terms. This causes the potential energy surfaces to meet at a glancing intersection rather than at the peak of a cone. Of the five possible Renner-Teller cases, HCNO^+ is an example of case (b) as defined by Lee *et al.*⁵⁹: both curves are repulsive as a function of bending but the two harmonic bending frequencies have the same value.

Following Worth and Cederbaum⁶⁰, for the two pairs of degenerate vibrational modes ($Q_{1/2}$ and $Q_{3/4}$), the vibronic coupling Renner-Teller Hamiltonian can be expressed as

$$\mathbf{H} = \frac{\omega}{2} (Q_i^2 + Q_j^2) + \begin{pmatrix} -\frac{1}{2}\gamma(Q_j^2 - Q_i^2) & \gamma Q_i Q_j \\ \gamma Q_i Q_j & \frac{1}{2}\gamma(Q_j^2 - Q_i^2) \end{pmatrix} \quad (4)$$

where ω is the degenerate vibrational frequency for the pair of modes i and j and γ is the parameter which causes splitting of the degenerate electronic surfaces. In this work the harmonic potential was replaced by polynomial functions but the RT γ parameters were retained.

The RT parameter ε can be used to describe the splitting and is defined as $V^\pm = V_m(1 \pm \varepsilon)$ where V_m is the mean potential of the split surfaces V^+ and V^- .⁶¹ The RT parameter can be calculated as

$$\varepsilon = \frac{V^+ - V^-}{V^+ + V^-}. \quad (5)$$

Usually only quadratic terms are considered, which for the fitting functions used here gives $\varepsilon = 2\gamma/\beta$ where β is the quadratic term parameter (see SI).

All parameters of the vibronic coupling Hamiltonian were obtained by least-squares fitting to the CASPT2 *ab initio* energies using the VCHAM package⁶² as implemented within the Quantics program suite⁶³. Fits were constrained so that the degenerate electronic energies and parameters for degenerate vibrational modes remained equal. Fitted parameters and plots comparing the *ab initio* energies to the vibronic coupling model are provided in the SI.

The photoelectron spectrum of fulminic acid was simulated in a similar manner to that described previously for both cyclobutadiene^{40,64} and phenol⁶⁵ from wavepacket dynamics simulations using the MCTDH method⁶⁶ implemented in Quantics⁶³. In this case, however, thermal effects were found to be important and a thermalised density operator was propagated in place of the usual 0 K wavepacket (see SI for 0 K spectra and assignments). Propagation was done including all 7 modes using a new multilayer implementation⁶⁷ of the ρ -MCTDH algorithm of Raab *et al.*⁶⁸.

The ground state nuclear density operator of neutral fulminic acid was obtained using energy relaxation⁶⁶ of an initial density operator built from harmonic oscillator eigenfunctions, thermalised to infinite temperature and propagated in imaginary time until the temperature was 300 K, the temperature of the experimental sample. A vertical excitation was then performed by placing the ground state neutral density operator on one of the two lowest electronic states of the fulminic acid cation and then propagating on these coupled states

for 200 fs. The photoelectron spectrum was obtained from the Fourier transform of the autocorrelation function as

$$I(\omega) \propto \omega \int_{-\infty}^{\infty} dt C(t) e^{i\omega t} e^{-(t/\tau)}, \quad (6)$$

where the last factor is an exponential dampening term to simulate experimental broadening in the photoelectron spectra. This phenomenological damping term accounts for missing terms in the model and experimental line broadening by convoluting the spectral lines with a Lorentzian function. The autocorrelation function $C(t)$ is defined as

$$C(t) = \text{Re} \{ \text{Tr} \rho_{s0} \} \quad (7)$$

where ρ_{s0} is the off-diagonal density matrix connecting the neutral ground-state with the initially excited cation state s . All seven vibrational modes were included in the calculation in a 3-layer multi-layer scheme,⁶⁹ adding basis functions until convergence with respect to the autocorrelation function was obtained. For all modes, the primitive basis functions were harmonic oscillator DVRs with 21 points used. Assignments in the photoelectron spectra to specific vibrational modes were determined by including/excluding modes from the simulation and observing the effect on the simulated spectrum.

The mechanism of the dissociation of the fulminic acid cation was calculated using the Gaussian-4 composite method⁷⁰ contained in the Gaussian09 program.⁷¹ The evaluated intermediates and transition states are based on the previous DFT calculations by Luna *et al.*²¹ Transition states were located by using the bery algorithm.⁷² They were identified by the presence of a vibration with an imaginary frequency, which corresponded to the respective reaction coordinate. The coordinates of all the intermediates and transition states are given in the SI (Tables S8 and S9). With these transition states the breakdown diagram is modeled using the minimalPEPICO program.⁷³

III. RESULTS AND DISCUSSION

A. Equilibrium Geometry and Harmonic Frequencies

Equilibrium bond lengths of $r_{\text{HC}} = 1.06$ (1.08), $r_{\text{CN}} = 1.17$ (1.17) and $r_{\text{NO}} = 1.21$ (1.21) Å were calculated for HCNO^+ , in good agreement with more elaborate calculations for the neutral molecule.¹⁷ Harmonic vibrational frequencies are given in Table I along with their symmetry labels (in C_{2v}). Values obtained by Mladenović and Lewerenz¹⁷ are also given for comparison. The force vectors of the normal modes are shown in the SI.

For the doubly degenerate H-C-N bend, lower levels of theory give imaginary frequencies, indicating that this geometry is not the global minimum. Many experimental^{18,23,28,30,31} and theoretical¹¹⁻¹⁵ studies have been carried out to determine whether the equilibrium structure of fulminic acid is linear or bent. As shown by Mladenović and Lewerenz¹⁷ and Bunker *et al.*,¹⁸ fulminic acid is a very floppy molecule with an almost flat region of the potential energy surface for hydrogen bending motions. Very large basis sets are required to converge to a

TABLE I. Comparison of harmonic vibrational frequencies with previous theoretical values of Mladenović and Lewerenz,¹⁷ "all" denotes that all electrons were correlated in the calculation. Units of cm^{-1} are employed.

Mode	CCSD(T)/cc-pVTZ (this work)	CCSD(T)/cc-pVQZ ¹⁷	CCSD(T)/cc-pVQZ ¹⁷ (all)	RCCSD(T)/cc-pVTZ (cation)	Description
$\omega_{1/2}(B_{1/2})$	206i	128i	33	677/512	H-C-N bend
$\omega_{3/4}(B_{1/2})$	555	555	565	402/368	C-N-O bend
$\omega_5(A_1)$	1266	1269	1279	1140	C-N-O sym. stretch
$\omega_6(A_1)$	2276	2280	2296	1992	C-N-O asym. stretch
$\omega_7(A_1)$	3500	3493	3505	3296	C-H stretch

linear equilibrium structure. Since we obtain cuts through the potential energy surface along the calculated normal modes, the precise determination of the equilibrium structure is not important here. As an aside, we note that in practical applications, fulminic acid is usually taken to have a linear structure, for example in determining its electronic and magnetic properties⁷⁴ or for describing collisions with other species.⁷⁵

For the cation, the harmonic stretching frequencies are broadly similar to the neutral. Values for the bending modes are seen not to be degenerate, only approximately so. Although as discussed above, the fulminic acid cation displays the Renner-Teller effect for the bending modes and thus a simple harmonic description is not sufficient, we retain harmonic frequencies for reference purposes. From least squares fits to the CASPT2 *ab initio* energies, we obtain γ parameter values (see Eq. 4) of 0.062959 and 0.0054112 eV for modes $\omega_{1/2}$ and $\omega_{3/4}$ respectively. Using Eq. 5 this gives RT parameters $|\epsilon|$ of 0.48 and 0.41 respectively, indicating a somewhat intermediate coupling strength compared to other RT systems⁶¹.

B. Photoelectron spectrum

Figure 1 shows the complete photoelectron spectrum. Four bands are observed at around 10.83 eV, 16.0 eV, 17.81 eV and 19.08 eV. The first, third and fourth band show well separated vibrational structure, while the second band is broad and unstructured. The spectrum agrees overall well with the previous dispersive photoelectron spectrum by Bastide *et al.*,³⁷ however due to the higher resolution additional bands are observed. Several narrow transitions appear that are assigned to ionization of H_2O and N_2 . They are indicated by asterisks in Figure 1.

Figure 2 shows the experimentally observed first band in more detail (black line), partial vibrational resolution is visible. From the first band an $\text{IE}_{ad} = 10.83 \pm 0.02$ eV is derived. The error bars are based on the full width of the band at half maximum. The value is in very good agreement with the previous one of 10.83 eV.³⁷ The main peak shows a shoulder on the high energy side and an irregular progression of multiple peaks is observed.

The red line in Figure 2 show the simulated photoelectron spectra obtained from MCTDH density operator dynamics run on the first two electronic states of the cation. The simulated spectrum has been normalised and shifted for best agreement with experiment. To represent the experimental broadening,



FIG. 1. Photoelectron spectrum of HCNO from 9 to 23 eV recorded at 30 eV photon energy. The signal upwards from 14.5 eV was multiplied by 5 for ease of viewing. Signals marked by asterisk are due to contamination from water (peak at 12.6 eV)⁷⁶ or molecular nitrogen (peaks at 15.6, 16.7, 16.9, 17.2 and 18.8 eV)⁷⁷.

an exponential damping term (see Eq. 6) was included in the computations, with a time constant of 100 fs. While the relative intensities are not fully accounted for in the simulated spectra, the peak positions in the experimental spectrum are well reproduced. To assign the spectrum, repeated runs starting at 0 K were made including different modes. Figure S12 in the supporting information shows the full and assigned 0 K spectrum compared to the one calculated at 300 K and the experimental spectrum. The simulations show that the first peak on the main band at 10.9 eV is caused by the CNO bending modes ω_3 and ω_4 . There is a small peak just below 11 eV which is due to the CNO symmetric stretching mode ω_5 . The two peaks at 11 and 11.05 eV are due to the RT modes ω_1 and ω_2 (approximate HCN bending). At higher energies there are some smaller peaks caused by stretching modes ω_6 and ω_7 (asymmetric CNO stretch and C-H stretch, respectively). A comparison between the 0 K and 300 K spectra shows that

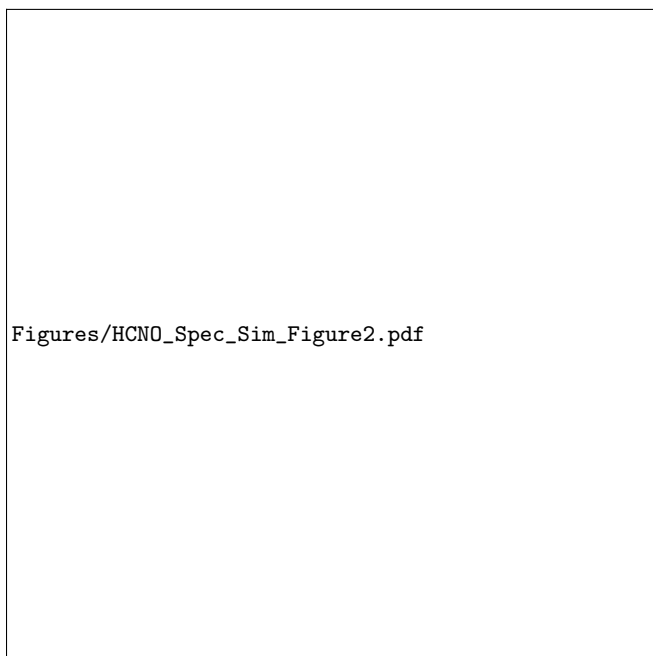


FIG. 2. Experimental photoelectron spectrum (black line) compared to the calculated spectrum (red). The simulated spectra has been normalised and shifted to match the main peak with experiment.

the shoulder on the high energy side of the main band is due to temperature allowing extra transitions in the $\omega_1 - \omega_4$ vibrations.

The second band, corresponding to the A^+ state of $HCNO^+$ ranges from 15.2 to 17.6 eV and is unstructured. A close-up is shown in the supporting information (Figure S2). The third band is shown in Figure 3 a). It features the intense origin band of the B^+ state at 17.81 eV and two further bands at +1130 and +2100 cm^{-1} above the origin. Additionally, a shoulder of around 240 cm^{-1} is visible for each band. The origin of the fourth band system (C^+ state, Figure 3 b)) lies at 19.08 eV. A well-resolved progression with a spacing of around 3000 cm^{-1} is apparent.

As mentioned above, a simulation of these progressions was not possible using the vibronic coupling model. However, a tentative assignment of the progressions is provided by investigating the involved orbitals. In Figure S4 the calculated MOs of $HCNO^+$ are shown. According to Bastide *et al.* the configuration of the neutral HCNO is $...6\sigma^27\sigma^21\pi^42\pi^4$.³⁷ For the B^+ state they assigned two vibrational bands with 1070 cm^{-1} and 2420 cm^{-1} to $\omega_s(CNO)$ and $\omega_{as}(CNO)$. In our spectrum a progression better described by a single mode is observed, so we assign it to the symmetric CNO stretch ω_5 , with a wavenumber of 1130 cm^{-1} in the excited state. This assignment is substantiated by the $2\sigma^*$ orbital (figure S4), corresponding to the 7σ orbital in the notation of Bastide *et al.*, which has strong CNO antibonding character. Thus removal of an electron from this MO is expected to lead to vibrational activity in a CNO mode.

The C^+ state shows a vibrational progression with 3150 cm^{-1} for the $v^+ = 1 \leftarrow v = 0$ fundamental. Transi-

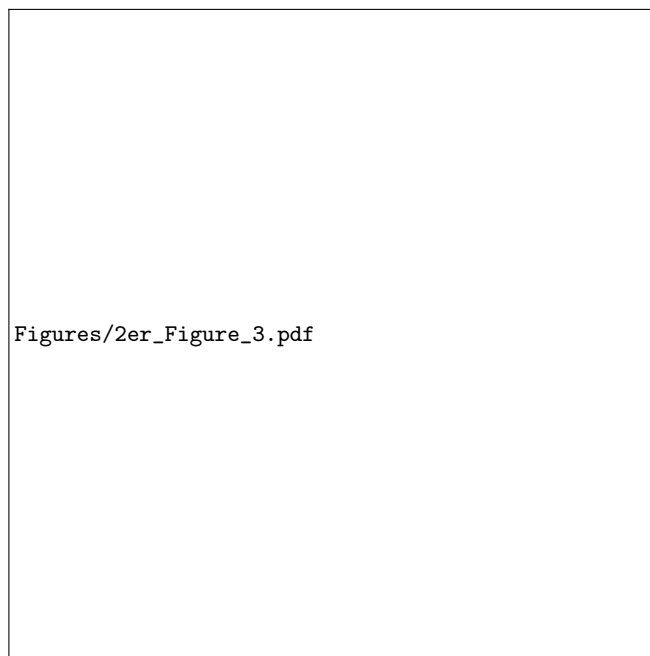


FIG. 3. High resolution spectra of the two excited states of HCNO with vibrational progression. a) shows in black the spectrum corresponding to the third band, b) shows the spectrum of the fourth band. The observed peaks are labeled with wavenumbers relative to the most intense peak.

tions into the first and second overtone at 6050 cm^{-1} and 8630 cm^{-1} are visible. Due to anharmonicity the energy difference between the peaks decreases. The high vibrational wavenumber indicates that the bands have to be assigned to a progression in the C-H-stretch mode $\omega_7(CH)$. The 2σ MO (figure S4, 6σ in Bastides notation³⁷) has C-H bonding character so a removal of that electron may destabilize the C-H bond and lead to vibrational activity in $\omega(CH)$. Nevertheless, it should be kept in mind that a simple Koopmans-type picture provides only a rather approximate description of the electronic structure that is not fully appropriate for HCNO.

C. Dissociative photoionization

The breakdown diagram for the dissociative photoionization of HCNO, recorded between 11.5 and 15.3 eV, is shown in Figure 4. The fractional abundances of the parent and daughter ion's TPE signal are plotted as a function of the photon energy. The open symbols represent experimental data. The simultaneously recorded TOF distribution show a small asymmetry for the daughter ion peaks, which indicates the presence of a kinetic shift (see Figure S3). As we consider the effect of the kinetic shift on the thermochemical quantities determined in the present work to be small, we did not include it in the data analysis.

The breakdown diagram shows several unusual features that are in contrast with a simple sequential dissociation in the ion. Until around 12.7 eV no fragmentation is visible,

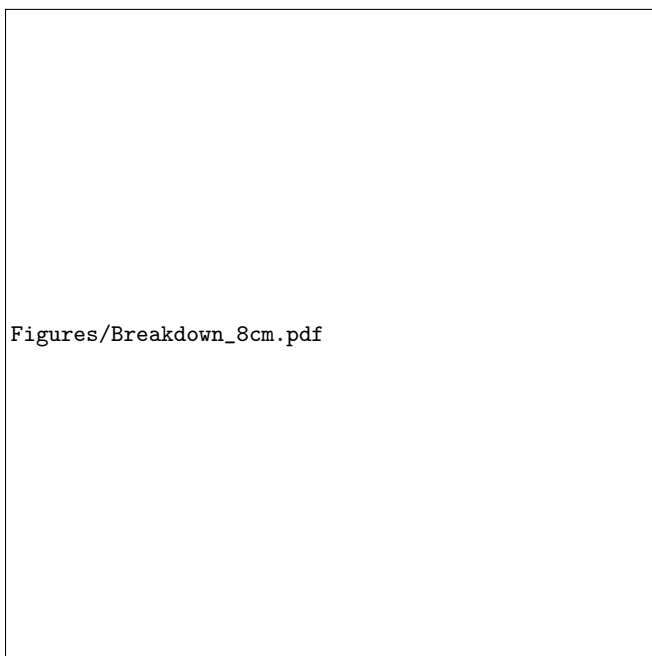


FIG. 4. Breakdown diagram of HCNO from 11.5 to 15.3 eV. The open symbols corresponds to the experimental data, while the solid lines are the fit produced by the minimalPEPICO program. The labeling of the curves show the m/z value as well as the assigned structure. The arrows show the appearance energies produced by the fit, which are also shown on the left.

TABLE II. Heats of reaction, $\Delta_R H$ for the dissociation $\text{HCNO} \rightarrow$ products. A more extensive table is available in the supporting information. The energies are taken from the Active thermochemical tables.⁷⁸ Ground state multiplicities are taken from ref.²¹.

Products	$\Delta_R H$ /eV
${}^1\text{HCO}^+ + {}^4\text{N}$	11.68
${}^3\text{NCO}^+ + {}^2\text{H}$	13.54
${}^2\text{NH}^+ + {}^1\text{CO}$	14.24
${}^1\text{NO}^+ + {}^2\text{CH}$	14.57
${}^3\text{CNO}^+ + {}^2\text{H}$	16.11

then the signal of m/z 29 (∇) increases, which corresponds to HCO^+ , while the parent signal (\square) drops to zero. At 13.45 eV, m/z 42 (\circ) starts to rise, maximizes at around 14 eV and decreases again. Interestingly the rise and decrease of m/z 42 are rather slow compared to HCO^+ . At this point, it is important to realize that the structure of m/z 42 is ambiguous and could correspond to CNO^+ or NCO^+ . Table II shows the heats of reaction $\Delta_R H$ of the most relevant fragment channels. They are calculated using the heats of formation provided by the Active Thermochemical Tables (ATcT).⁷⁹ Assuming a barrierless mechanism, these reaction enthalpies are equivalent to appearance energies. In any case $\Delta_R H$ represent the minimum energy that is required to produce these ions. In fact, HCO^+ appears above the computed value of 11.68 eV. The heat of reaction for formation of $\text{CNO}^+ + \text{H}$, the presumed carrier of

$m/z = 42$, is $\Delta_R H = 16.11$ eV, outside the energy range monitored in Figure 4. However, for the product channel ${}^3\text{NCO}^+ + {}^2\text{H}$ $\Delta_R H = 13.54$ eV is computed, a thermochemical value that agrees well with the observed onset. We therefore conclude an isomerization on the ionic potential energy surface. The second unusual feature corresponds to the HCO^+ curve (∇), which drops to almost zero at 13.9 eV, but rises again to a value of around 12% of its maximum at 14.5 eV. This suggest two different channels for the formation of this fragment. Two further fragments are visible, the formation of $m/z = 15$ (\times), corresponding to NH^+ at 14.1 eV, and the onset of $m/z = 30$ NO^+ (\triangle) around 14.5 eV. Both fragment ion curves are in accordance with the values in Table II.

The minimalPEPICO program allows the modeling of these breakdown diagrams to extract thermochemical data.⁷³ This requires detailed knowledge of the reaction mechanism that form the products and the vibrational frequencies of the stationary points of the potential energy surface. Luna *et al.* published the global potential energy surface of the $[\text{H},\text{N},\text{C},\text{O}]^+$ system in doublet and quartet multiplicity, including transition states. Their findings yield the mechanism shown in Figure 5, which was confirmed by our own calculations that yielded the necessary frequencies. The appearance of HCO^+ requires the formation of a C-O bond which is not present in the parent HCNO^+ . This bond can form via **TS1** where the C-N-O angle is decreased to 97.6, which leads to the structure **I**. Formation of HCO^+ also produces atomic nitrogen. The ground state of N is ${}^4\text{S}_{3/2}$.⁸⁰ Since the parent ion is of doublet multiplicity, the direct formation of $\text{HCO}^+ + {}^4\text{N}$ is not possible and the cation has to switch to the quartet surface since the product channel $\text{HCO}^+ + {}^2\text{N}$ lies at 14.1 eV. We propose that that this happens either at **I** or between **I** and the products. On the quartet surface **I** may dissociate over **TS2** and molecule-ion complex **II**.²¹ Note that in the experiment we only measure the highest barrier along the reaction coordinate. This mechanism can also explain the revival of HCO^+ at around 14.0 eV. At this energy the reaction along the doublet surface is possible to form $\text{HCO}^+ + {}^2\text{N}$ (figure 5) via **TS3** and the HCON^+ intermediate.²¹ The formation of NCO^+ requires the formation of the isocyanic acid cation HNCO^+ . This mechanism involves a 1,2-H-shift (**TS4**) to **III** and an N-O bond cleavage (**TS5**). The solid lines in Figure 4 represent the fit obtained using the MinimalPEPICO program employing the highest barriers (TS1 to $\text{HCO}^+ + {}^2\text{N}$, TS4 to $\text{NCO}^+ + {}^2\text{H}$) of the above mechanism. As visible, the behavior of m/z 29 and the onset of m/z 42 are well represented. Zero Kelvin appearance energies for both fragments are derived from the model, $AE_{0K}(\text{HCNO}, \text{HCO}^+) = 13.0 \pm 0.1$ eV and $AE_{0K}(\text{HCNO}, \text{NCO}^+) = 13.5 \pm 0.1$ eV. The reaction coordinate for formation of NO^+ and NH^+ has not been investigated, consequently their appearance energies are not modeled in this work. The observed onset of NCO^+ agrees very well with the ATcT value, while the $AE_{0K}(\text{HCNO}, \text{HCO}^+)$ is associated with a complex doublet-quartet intersystem crossing. This ISC may be close to **TS1** or **I** (Figure 5) and does not allow an extraction of the $\Delta_R H$.

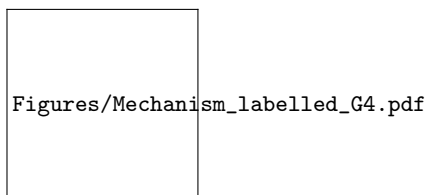


FIG. 5. Mechanism of the isomerization of the HCNO cation to form ${}^3\text{NCO}^+$ and ${}^1\text{HCO}^+$. Energies are given in eV relative to the neutral HCNO molecule. Values marked with ^a were calculated using the G4 composite method. Values marked with ^b and ^c were taken from Ref.²¹ and from the Active Thermochemical Tables⁷⁸, respectively. Lines shown in black are on the doublet surface and lines in red are on the quartet surface.

IV. CONCLUSION

The VUV spectroscopy of fulminic acid, HCNO, has been investigated using synchrotron radiation and dispersive as well as threshold photoelectron detection. Compared to a previous spectrum³⁷ the present spectra are better resolved and show more information. Four bands are observed, three of them exhibit a vibrational progression. The band origins are identified at 10.83 ± 0.02 eV ($X^{+2}\Pi$) 17.81 ± 0.01 eV (B^+) and 19.08 ± 0.03 eV (C^+), respectively. A simulation of the transition into the Renner-Teller distorted $X^{+2}\Pi$ ground state of the cation using wavepacket dynamics that rely on a vibronic coupling Hamiltonian yielded very good agreement with the experiment. Several bending mode transitions are identified in the simulations. In addition, hot and sequence band transitions from low energy bending modes of neutral HCNO are essential to achieve agreement between experiment and simulation. No simple description of the transitions into excited electronic states of cation is possible, because twelve electronic states contribute to the transitions and the excited state potential energy surfaces depend in a complicated way on the normal mode coordinates. Therefore only an approximate character was assigned to the transitions, which can nevertheless qualitatively explain the observed vibronic transitions.

Furthermore, a breakdown diagram of HCNO up to 15.3 eV was recorded to investigate its dissociative photoionisation. The spectrum was then modelled to extract thermochemical data and the mechanism has been investigated computationally. Dissociative ionization to ${}^1\text{HCO}^+ + {}^4\text{N}$ was found to be the lowest energy dissociation pathway with an appearance energy of $AE_{0K}(\text{HCNO}, \text{HCO}^+) = 13.0 \pm 0.1$ eV. The reaction requires a switch to the quartet potential energy surface in the cation. Next, dissociation to ${}^3\text{NCO}^+ + {}^2\text{H}$ sets in at $AE_{0K}(\text{HCNO}, \text{NCO}^+) = 13.5 \pm 0.1$ eV. This dissociation is preceded by an isomerization from HCNO^+ to HNCO^+ , which proceeds via a tricyclic intermediate. The confirmation of isomerization from HCNO^+ to HNCO^+ might be relevant for explaining the relative abundance of the various CHNO isomers and their fragments, which is not well understood.⁸¹

V. SUPPORTING INFORMATION

See supporting information for additional experimental and computational information.

VI. DATA AVAILABILITY STATEMENT

The data that supports the findings of this study are available within the article and its supporting information. Further data are available from the authors upon request.

ACKNOWLEDGMENTS

The photoelectron spectra were recorded at the PLEIADES beamline at Synchrotron SOLEIL, France, proposal 20200183. We thank E. Robert for technical assistance and the SOLEIL staff for operation of the equipment and storage ring during the experiments. The dissociative photoionization was investigated at the VUV beamline of the Swiss Light Source, Villigen/CH. The work was funded by the Deutsche Forschungsgemeinschaft, contract FI575/13-2. BPM and GW acknowledge financial support from the UK Engineering and Physical Science Research Council (EPSRC) Grant No. EP/T006560/1.

¹F. Kurzer, *J. Chem. Educ.* **77**, 851 (2000).

²C. Wentrup, *Angew. Chem. Int. Ed.* **58**, 14800 (2019), <https://onlinelibrary.wiley.com/doi/pdf/10.1002/anie.201906356>.

³N. Marcelino, J. Cernicharo, B. Tercero, and E. Roueff, *Astrophys. J.* **690**, L27 (2009).

⁴N. Marcelino, S. Brünken, J. Cernicharo, D. Quan, E. Roueff, E. Herbst, and P. Thaddeus, *Astron. Astrophys.* **516**, A105 (2010).

⁵E. Mendoza, B. Lefloch, A. Lopez-Sepulcre, C. Ceccarelli, C. Codella, H. M. Boechat-Roberty, and R. Bachiller, *Mon. Not. R. Astron. Soc.* **445**, 151 (2014).

⁶B. Lefloch, R. Bachiller, C. Ceccarelli, J. Cernicharo, C. Codella, A. Fuente, C. Kahane, A. López-Sepulcre, M. Tafalla, C. Vastel, E. Caux, M. González-García, E. Bianchi, A. Gómez-Ruiz, J. Holdship, E. Mendoza, J. Ospina-Zamudio, L. Podio, D. Quénard, E. Roueff, N. Sakai, S. Viti, S. Yamamoto, K. Yoshida, C. Favre, T. Monfredini, H. M. Quitián-Lara, N. Marcelino, H. M. Boechat-Roberty, and S. Cabrit, *Monthly Notices of the Royal Astronomical Society* **477**, 4792 (2018).

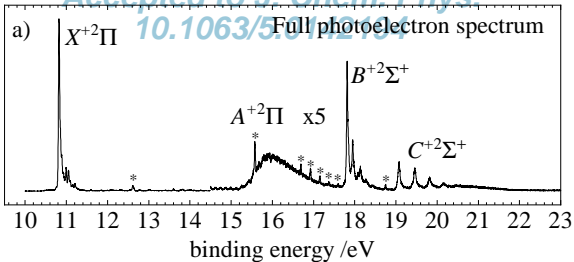
⁷N. Marcelino, M. Agúndez, J. Cernicharo, E. Roueff, and M. Tafalla, *Astron. Astrophys.* **612**, L10 (2018).

⁸M. Agúndez, N. Marcelino, J. Cernicharo, E. Roueff, and M. Tafalla, *Astron. Astrophys.* **625**, A147 (2019).

- ⁹D. H. Quan, E. Herbst, Y. Osamura, and E. Roueff, *Astrophys. J.* **725**, 2101 (2010).
- ¹⁰S. Brünken, A. Belloche, S. Martín, L. Verheyen, and K. M. Menten, *Astron. Astrophys.* **516**, A109 (2010).
- ¹¹M. S. Schuurman, S. R. Muir, W. D. Allen, and H. F. Schaefer III, *J. Chem. Phys.* **120**, 11586 (2004).
- ¹²M. T. Nguyen, K. Pierloot, and L. G. Vanquickenborne, *Chem. Phys. Lett.* **181**, 83 (1991).
- ¹³A. P. Rendell, T. J. Lee, and R. Lindh, *Chem. Phys. Lett.* **194**, 84 (1992).
- ¹⁴N. Pinnavaia, M. J. Bramley, M. D. Su, W. H. Green, and N. C. Handy, *Mol. Phys.* **78**, 319 (1993).
- ¹⁵J. Koput, B. P. Winnewisser, and M. Winnewisser, *Chem. Phys. Lett.* **255**, 357 (1996).
- ¹⁶A. M. Mebel, A. Luna, M. C. Lin, and K. Morokuma, *J. Chem. Phys.* **105**, 6439 (1996).
- ¹⁷M. Mladenović and M. Lewerenz, *Chem. Phys.* **343**, 129 (2008).
- ¹⁸P. R. Bunker, B. M. Landsberg, and B. P. Winnewisser, *Journal of Molecular Spectroscopy* **74**, 9 (1979).
- ¹⁹P. R. Bunker, *Annual Review of Physical Chemistry* **34**, 59 (1983).
- ²⁰R. Mondal and D. Debasis Mukhopadhyay, *Int. J. Quantum Chem.* **120**, e26195 (2020).
- ²¹A. Luna, A. M. Mebel, and K. Morokuma, *J. Chem. Phys.* **105**, 3187 (1996).
- ²²M. Winnewisser and H. K. Bodenseh, *Zeitschrift für Naturforschung A* **22a**, 1724 (1967).
- ²³B. P. Winnewisser, M. Winnewisser, and F. Winther, *J. Mol. Spectrosc.* **51**, 65 (1974).
- ²⁴B. P. Winnewisser, M. Winnewisser, G. Wagner, and J. Preusser, *J. Mol. Spectrosc.* **142**, 29 (1990).
- ²⁵W. Beck and K. Feldl, *Angew. Chem.* **78**, 746 (1966).
- ²⁶B. P. Winnewisser and M. Winnewisser, *Journal of Molecular Spectroscopy* **29**, 505 (1969).
- ²⁷W. Beck, P. Swoboda, K. Feldl, and R. S. Tobias, *Chem. Ber.* **104**, 533 (1971).
- ²⁸E. L. Ferretti and K. Narahari Rao, *J. Mol. Struct.* **51**, 97 (1974).
- ²⁹V. E. Bondybey, J. H. English, C. W. Mathews, and R. J. Contolini, *J. Mol. Spectrosc.* **92**, 431 (1982).
- ³⁰B. P. Winnewisser and P. Jensen, *J. Mol. Spectrosc.* **101**, 408 (1983).
- ³¹S. Albert, M. Winnewisser, and B. P. Winnewisser, *Ber. Bunsenges.* **100**, 1876 (1996).
- ³²S. Albert, K. K. Albert, M. Winnewisser, and B. P. Winnewisser, *J. Mol. Struct.* **599**, 347 (2001).
- ³³W. Feng and J. F. Hershberger, *J. Phys. Chem. A* **118**, 829 (2014).
- ³⁴W. Feng and J. F. Hershberger, *Chem. Phys.* **472**, 18 (2016).
- ³⁵W. Feng, J. P. Meyer, and J. F. Hershberger, *J. Phys. Chem. A* **110**, 4458 (2006).
- ³⁶M. Gerlach, T. Preitschopf, E. Karaev, H. M. Quitoán-Lara, D. Mayer, J. Bozek, I. Fischer, and R. F. Fink, *Phys. Chem. Chem. Phys.* **24**, 15217 (2022).
- ³⁷J. Bastide and J. P. Maier, *Chem. Phys.* **12**, 177 (1976).
- ³⁸C. E. C. A. Hop, K. J. Van den Berg, J. L. Holmes, and J. K. Terlouw, *J. Am. Chem. Soc.* **111**, 72 (1989).
- ³⁹I. Fischer and S. T. Pratt, *Phys. Chem. Chem. Phys.* **24**, 1944 (2022).
- ⁴⁰L. Bosse, B. P. Mant, D. Schleier, M. Gerlach, I. Fischer, A. Krueger, P. Hemberger, and G. Worth, *J. Phys. Chem. Lett.* **12**, 6901 (2021).
- ⁴¹F. Holzmeier, M. Lang, I. Fischer, X. Tang, B. Cunha de Miranda, C. Romanzin, C. Alcaraz, and P. Hemberger, *J. Chem. Phys.* **142**, 184306 (2015).
- ⁴²F. Holzmeier, T. J. A. Wolf, C. Gienger, I. Wagner, J. Bozek, S. Nandi, C. Nicolas, I. Fischer, M. Gühr, and R. F. Fink, *J. Chem. Phys.* **149**, 034308 (2018).
- ⁴³<https://www.synchrotron-soleil.fr/fr/lignes-de-lumiere/pleiades> (2019).
- ⁴⁴M. Johnson, A. Bodi, L. Schulz, and T. Gerber, *Nucl. Instrum. Methods Phys. Res. Sect. A* **610**, 597 (2009).
- ⁴⁵C. Wentrup, B. Gerech, and H. Brielh, *Angew. Chem. Int. Ed.* **18**, 467 (1979).
- ⁴⁶B. Sztaray, K. Voronova, K. G. Torma, K. J. Covert, A. Bodi, P. Hemberger, T. Gerber, and D. L. Osborn, *J. Chem. Phys.* **147**, 013944 (2017).
- ⁴⁷B. Sztaray and T. Baer, *Rev. Sci. Instrum.* **74**, 3763 (2003).
- ⁴⁸H.-J. Werner, P. J. Knowles, G. Knizia, F. R. Manby, and M. Schütz, *WIREs Comput. Mol. Sci.* **2**, 242 (2012).
- ⁴⁹H.-J. Werner, P. J. Knowles, G. Knizia, F. R. Manby, M. Schütz, *et al.*, (2019), see <https://www.molpro.net>.
- ⁵⁰H.-J. Werner, P. J. Knowles, F. R. Manby, J. A. Black, K. Doll, A. Heßelmann, A. Kats, T. Köhn, A. Korona, D. A. Kreplin, Q. Ma, T. F. Miller III, A. Mitrushchenkov, K. A. Peterson, I. Polyak, G. Rauhut, and M. Sibaev, *J. Chem. Phys.* **152**, 144107 (2020).
- ⁵¹M. J. O. Deegan and P. J. Knowles, *Chem. Phys. Lett.* **227**, 321 (1994).
- ⁵²T. H. Dunning Jr, *J. Chem. Phys.* **90**, 1007 (1989).
- ⁵³J. D. Watts, J. Gauss, and R. J. Bartlett, *J. Chem. Phys.* **98**, 8718 (1993).
- ⁵⁴I. F. Galván, M. Vacher, A. Alavi, C. Angeli, F. Aquilante, J. Autschbach, J. J. Bao, S. I. Bokarev, N. A. Bogdanov, R. K. Carlson, L. F. Chibotaru, J. Creutzberg, N. Dattani, M. G. Delcey, S. S. Dong, A. Dreuw, L. Freitag, L. M. Frutos, L. Gagliardi, F. Gendron, A. Giussani, L. González, G. Grell, M. Guo, C. E. Hoyer, M. Johansson, S. Keller, S. Knecht, G. Kovačević, E. Källman, G. Li Manni, M. Lundberg, Y. Ma, S. Mai, J. P. Malhado, P. Å. Malmqvist, P. Marquetand, S. A. Mewes, J. Norell, M. Olivucci, M. Oppel, Q. M. Phung, K. Pierloot, F. Plasser, M. Reiher, A. M. Sand, I. Schapiro, P. Sharma, C. J. Stein, L. K. Sørensen, D. G. Truhlar, M. Ugandi, L. Ungur, A. Valentini, S. Vancoillie, V. Veryazov, O. Weser, T. A. Wesolowski, P.-O. Widmark, S. Wouters, A. Zech, J. P. Zobel, and R. Lindh, *J. Chem. Theory Comput.* **15**, 5925 (2019).
- ⁵⁵P.-Å. Malmqvist, A. Rendell, and B. O. Roos, *J. Phys. Chem.* **94**, 5477 (1990).
- ⁵⁶P.-Å. Malmqvist, K. Pierloot, A. R. M. Shahi, C. J. Cramer, and L. Gagliardi, *J. Chem. Phys.* **128**, 204109 (2008).
- ⁵⁷V. Sauri, L. Serrano-Andrés, A. R. M. Shahi, G. L. S. Vancoillie, and K. Pierloot, *J. Chem. Theory Comput.* **7**, 153 (2011).
- ⁵⁸H. Köppel, W. Domcke, and L. S. Cederbaum, *Adv. Chem. Phys.* **57**, 59 (1984).
- ⁵⁹T. J. Lee, D. J. Fox, and H. F. Schaefer III, *J. Chem. Phys.* **81**, 356 (1984).
- ⁶⁰G. A. Worth and L. S. Cederbaum, *Annu. Rev. Phys. Chem.* **55**, 127 (2004).
- ⁶¹Q. Lu, *ACS Omega* **7**, 44078 (2022).
- ⁶²G. A. Worth, K. Giri, G. W. Richings, I. Burghardt, M. H. Beck, A. Jäckle, and H.-D. Meyer, *The Quantics Package Version 2.0*. See <http://www.chem.ucl.ac.uk/quantics>, University College London, U.K. (2020).
- ⁶³G. A. Worth, *Comput. Phys. Commun.* **248**, 107040 (2020).
- ⁶⁴S. Saddique and G. A. Worth, *Chem. Phys.* **329**, 99 (2006).
- ⁶⁵M. P. Taylor and G. A. Worth, *Chem. Phys.* **515**, 719 (2018).
- ⁶⁶M. H. Beck, A. Jäckle, G. A. Worth, and H.-D. Meyer, *Phys. Rep.* **324**, 1 (2000).
- ⁶⁷A. Van Haefen, C. Ash, and G. A. Worth, *J. Chem. Phys.* **xxx**, xxx (2023), To be submitted.
- ⁶⁸A. Raab, I. Burghardt, and H.-D. Meyer, *J. Chem. Phys.* **111**, 8759 (1999).
- ⁶⁹O. Vendrell and H.-D. Meyer, *J. Chem. Phys.* **134**, 44135 (2011).
- ⁷⁰L. A. Curtiss, P. C. Redfern, and K. Raghavachari, *J. Chem. Phys.* **126**, 084108 (2007).
- ⁷¹M. J. Frisch, G. W. Trucks, H. B. Schlegel, G. E. Scuseria, M. A. Robb, J. R. Cheeseman, G. Scalmani, V. Barone, B. Mennucci, G. A. Petersson, H. Nakatsuji, M. Caricato, X. Li, H. P. Hratchian, A. F. Izmaylov, J. Bloino, G. Zheng, J. L. Sonnenberg, M. Hada, M. Ehara, K. Toyota, R. Fukuda, J. Hasegawa, M. Ishida, T. Nakajima, Y. Honda, O. Kitao, H. Nakai, T. Vreven, J. A. Montgomery Jr., J. E. Peralta, F. Ogliaro, M. Bearpark, J. J. Heyd, E. Brothers, K. N. Kudin, V. N. Staroverov, R. Kobayashi, J. Normand, K. Raghavachari, A. Rendell, J. C. Burant, S. S. Iyengar, J. Tomasi, M. Cossi, N. Rega, J. M. Millam, M. Klene, J. E. Knox, J. B. Cross, V. Bakken, C. Adamo, J. Jaramillo, R. Gomperts, R. E. Stratmann, O. Yazyev, A. J. Austin, R. Cammi, C. Pomelli, J. W. Ochterski, R. L. Martin, K. Morokuma, V. G. Zakrzewski, G. A. Voth, P. Salvador, J. J. Dannenberg, S. Dapprich, A. D. Daniels, Ö. Farkas, J. B. Foresman, J. V. Ortiz, J. Cioslowski, and D. J. Fox, *Gaussian 16, Revision B.01* (Gaussian, Inc., Wallingford CT, 2016).
- ⁷²H. B. Schlegel, *J. Comp. Chem.* **3**, 214 (1982).
- ⁷³B. Sztaray, A. Bodi, and T. Baer, *J. Mass. Spectrom.* **45**, 1233 (2010).
- ⁷⁴M. Mladenović, M. Elhiyani, and M. Lewerenz, *J. Chem. Phys.* **131**, 034302 (2009).
- ⁷⁵A. Naindoubaa, C. Nkema, Y. Ajilib, K. Hammamib, N. Gotouma, and L. C. Owono Owonoa, *Chem. Phys. Lett.* **636**, 67 (2015).
- ⁷⁶J. E. Reutt, L. S. Wang, Y. T. Lee, and D. A. Shirley, *J. Chem. Phys.* **85**, 6928 (1986).

- ⁷⁷J. W. Rabalais, T. P. Debies, J. L. Berkosky, J. J. Huang, and F. O. Ellison, *J. Chem. Phys.* **61**, 516 (1974).
- ⁷⁸B. Ruscic and D. H. Bross, Active Thermochemical Tables (ATcT) values based on ver. 1.122r of the Thermochemical Network (2021); available at [ATcT.anl.gov](https://atct.anl.gov).
- ⁷⁹B. Ruscic, R. E. Pinzon, G. von Laszewski, D. Kodeboyina, A. Burcat, D. Leahy, D. Montoy, and A. F. Wagner, *J. Phys.: Conference Series* **16**, 561 (2005).
- ⁸⁰A. Kramida, Yu. Ralchenko, J. Reader, and NIST ASD Team, NIST Atomic Spectra Database (ver. 5.9), [Online]. Available: <https://physics.nist.gov/asd> [2022, August 31]. National Institute of Standards and Technology, Gaithersburg, MD. (2021).
- ⁸¹A. Jiménez-Escobar, B. M. Giuliano, G. M. Muñoz Caro, J. Cernicharo, and N. Marcelino, *The Astrophysical Journal* **788**, 19 (2014).

photoelectron signal



Binding energy /eV

10.8

10.9

11.0

11.1

11.2

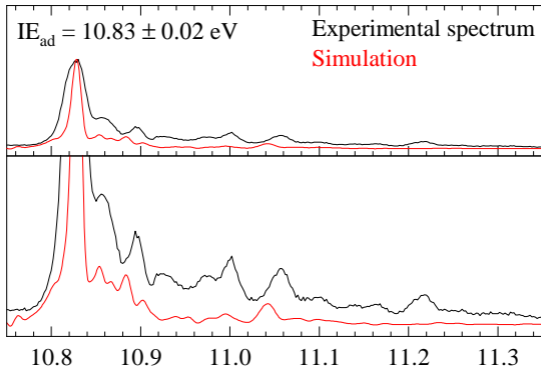
11.3

$IE_{ad} = 10.83 \pm 0.02$ eV

Experimental spectrum

Simulation

photoelectron signal



Binding energy /eV

photoelectron signal

